Beta decay of ^{21}O

D. E. Alburger, C. J. Lister,* J. W. Olness, and D. J. Millener
Brookhaven National Laboratory, Upton, New York 11973
(Received 8 December 1980)

The radioisotope ^{21}O was produced in the $^{9}Be(^{18}O,2p\alpha)^{21}O$ reaction using 80–110-MeV ^{18}O ions. Activities emerging from a Be target foil were stopped in a He gas cell and transferred to a counting area where γ and β rays were measured using Ge(Li) and plastic detectors. Thirteen γ rays were observed in singles, γ-γ, or β-γ coincidence measurements following the β decay of ^{21}O to known excited states of ^{21}F at 1730, 3460, 3518, (3639), 4572, and 4584 keV. Detailed information on the properties of the ^{21}F energy levels was obtained. By stopping the gas flow and measuring the decay of γ rays, the half-life of ^{21}O was found to be 3.42 ± 0.10 sec. β end-point energies measured by β-γ coincidences lead to a mass excess of 8105 ± 175 keV for ^{21}O in agreement with more accurate reaction Q values. Detailed shell-model calculations were carried out and reproduce the main features of the ^{21}O decay scheme.

[RADIOACTIVITY ^{21}O: measured E_γ, I_γ, E_β, I_β, γ-γ, and β-γ coin., $T_{1/2}$; gas transfer, Ge(Li) and plastic detectors; deduced ^{21}O decay, scheme, logft values; compared with theory.]

I. INTRODUCTION

^{21}O is a $T_z = +\frac{5}{2}$ nucleus and is one of a series of eight such nuclei in the *sd* shell extending from ^{21}O to ^{35}P. During the past decade, studies of this sequence have been made[1] in order to determine the masses, half-lives, and spectroscopic properties of these nuclei. Although ^{21}O is the only one of the series whose β decay has not been reported previously, there have been several three-neutron transfer reaction measurements leading to values for the ^{21}O mass excess. In particular, Artukh *et al.*[2] found a value of $9.3^{+0.3}_{-0.7}$ MeV for the ^{21}O mass excess, about 1.2 MeV higher than the later concordant values obtained by Ball *et al.*[3,4] using the reaction $^{208}Pb(^{18}O, ^{21}O)^{205}Pb$ and by Naulin *et al.*[5] using the reaction $^{18}O(^{18}O, ^{15}O)^{21}O$. A weighted mean value of 8126 ± 51 keV for the ^{21}O mass excess may be derived from these latter two reports.

The mass excess of the ^{21}F daughter nucleus is -47 keV (Ref. 6), and the total β decay energy of ^{21}O is thus 8173 keV. It might therefore be expected that numerous excited states in ^{21}F could be populated by ^{21}O β-ray branching and that detailed information could be obtained on the structure of these ^{21}F levels. In some earlier searches for ^{21}O at Brookhaven,[1] the expectations as to the decay properties of this isotope were guided by the work of Lanford and Wildenthal.[7] Their calculations indicated that ^{21}O should have a spin-parity of $J^\pi = \frac{5}{2}^+$ and that the principal β-ray branch should lead to a $J^\pi = \frac{3}{2}^+$ excited state in ^{21}F, predicted to be at 1560 keV, with logft = 5.44. β-ray branching to the $\frac{5}{2}^+$ ground state was predicted to be weak (logft = 8.41), but another major branch, to a $J = \frac{5}{2}$ state at 3.23 MeV (logft = 4.89), should also take place. Based on the decay energy derived from the mass excess expected[8] for ^{21}O, and the calculated decay scheme, the estimate for the half-life of ^{21}O was 1.2 sec.

The energy level scheme of ^{21}F, first studied by Hinds *et al.*[9] via the $^{19}F(t,p)^{21}F$ reaction, was later reinvestigated by Warburton and Olness,[10] who also measured the ^{21}F deexcitation γ rays produced in this reaction. For those levels of ^{21}F below 3 MeV, more accurate excitation energies were obtained, as well as restrictions on the spins and parities of some of the states. In the vicinity of the $\frac{3}{2}^+$ state predicted at 1560 keV by Lanford and Wildenthal, the possible candidates were ^{21}F levels with energies of 1729.6 ± 1.0 and 1754.9 ± 0.7 keV. The first of these was limited experimentally to $J^\pi = (\frac{1}{2}^+)$, $\frac{3}{2}$, or $(\frac{5}{2}^+)$, with $\frac{3}{2}$ preferred, while no restrictions were placed on the second. These states were shown to decay 82% and 100%, respectively, to the ground state by γ-ray emission. Thus, on the assumption that the 1729.6-keV state was the $J^\pi = \frac{3}{2}^+$ level expected from the calculation,[7] an obvious signature of ^{21}O β decay would be the emission of a fast-decaying γ ray of 1729.6 keV. Preliminary theoretical calculations by one of us (D.J.M.) during the early part of the present work confirmed that the 1729.6-keV state was very probably the expected $J^\pi = \frac{3}{2}^+$ level. (In order to provide a convenient reference for the subsequent presentation, the energy level scheme for ^{21}F given in Fig. 1 represents a synthesis of the present and previous results.)

Numerous previous attempts have been made at this laboratory since 1972 to produce and identify ^{21}O (see Ref. 1 for a summary). In one of these experiments the $^{9}Be(^{18}O, 2p\alpha)^{21}O$ reaction was tried at $E(^{18}O) = 77$ MeV using a gas sweeping system originally designed for a study[11] of ^{25}Ne and

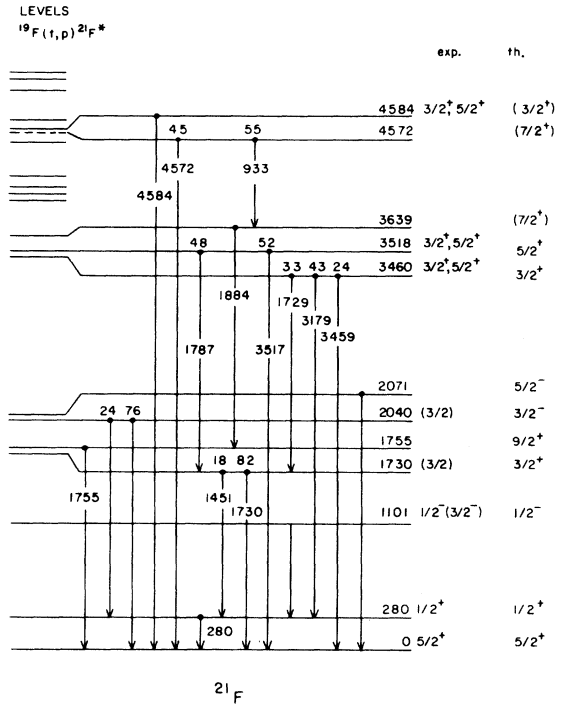

FIG. 1. Energy level scheme for ^{21}F, synthesized from previous data together with data from the present work. See also Table I.

similar in some respects to that of the current work. However, in this as well as all the other attempts to find ^{21}O, there were persistent background problems, the most serious of which was the production of ^{24}Na radioactivity of 15 h half-life. The double-escape peak of the ^{24}Na 2754-keV γ ray has an energy of 1732 keV, and in the spectrum from a Ge(Li) detector this peak always hindered the search for a fast-decaying ^{21}O peak of 1730 keV.

The present observation of ^{21}O β decay following the $^{9}Be(^{18}O, 2p\alpha)^{21}O$ reaction, and the detailed study of the structure of the ^{21}F energy levels reported herein, was made possible by several factors. One was an effective scheme for removing the ^{24}Na background by using a filter of a general type devised by Davids[12] for a different application at Argonne National Laboratory. Another factor was the realization, through fusion-evaporation reaction calculations, that a much greater yield of ^{21}O in the reaction $^{9}Be(^{18}O, 2p\alpha)^{21}O$ would occur at ^{18}O beam energies $\gtrsim$100 MeV. Finally, considerable improvements in yield resulted from optimization of parameters (dimensions, pressures, etc.) in the gas sweeping system. Some of these considerations are reported in the Appendix.

II. EXPERIMENTAL METHODS

The experimental arrangement for the production of ^{21}O and the measurement of its radiations is shown schematically in Fig. 2. A beam of ^{18}O ions (in charge states 6^+ or 7^+) from the MP Tandem Van de Graaff accelerator was collimated to a diameter of 3 mm and allowed to fall on a Be foil target 0.025 mm thick which also served as the entrance window of a gas cell made of glass. Reaction products from the Be foil were stopped in helium gas which was introduced near the target foil at a pressure of about 1.8 atm and carried the activity out the other end of the cell through a 1.67-mm i.d. plastic tubing. The length of the cell was 13 cm, sufficient, with the helium pressure used, to stop the most energetic ^{21}O recoil particles produced in the Be foil. A Ta stop kept the beam from damaging the plastic tubing. After passing ~4 m from the target room through a shielding wall to the counting area, the tubing brought the activity to a filter (see Appendix) for absorption of the ^{24}Na activity. The gas was then passed through a heated coil of stainless steel tubing of 1.6 mm i.d. which reduced the various fluorine activities whose γ rays gave a Compton background in the 1–3 MeV region. Oxygen activities were finally trapped out of the gas in a cylindrical aluminum cell of 5 cm i.d. and 6 mm height, having top and bottom Al covers 0.8 mm thick. This was filled with silica gel. The entrance and exit regions of the cell were flared and covered with mesh so as to improve the gas-flow characteristics. Tests on the performance of the counting cell, as well as the overall system, were conveniently made on the γ rays from both ^{19}O and ^{20}O, which are produced in considerable intensities, presumably via one-neutron and two-neutron transfer reactions. The final exit of the system was connected to a mechanical pump.

As shown in Fig. 2, two electrically activated gas valves were provided on either side of the counting cell to stop the gas flow, thereby allowing the measurement of the decay rates of γ rays from activities fixed in the cell. The valves were operated on command from a timer-programmer[13] which also controlled the routing of data storage in the Σ-7 computer.

For the detection of γ and β radiations from ^{21}O, standard Ge(Li) and plastic scintillators were placed on either side of the counting cell with 6 mm of brass to exclude β rays from the Ge(Li) detector. Because of the greater concentration of activity near the entrance to the cell, an improved yield was obtained by displacing the detectors 1.5 cm toward the entrance as indicated in Fig. 2. Two Ge(Li) detectors of 18% and 22%

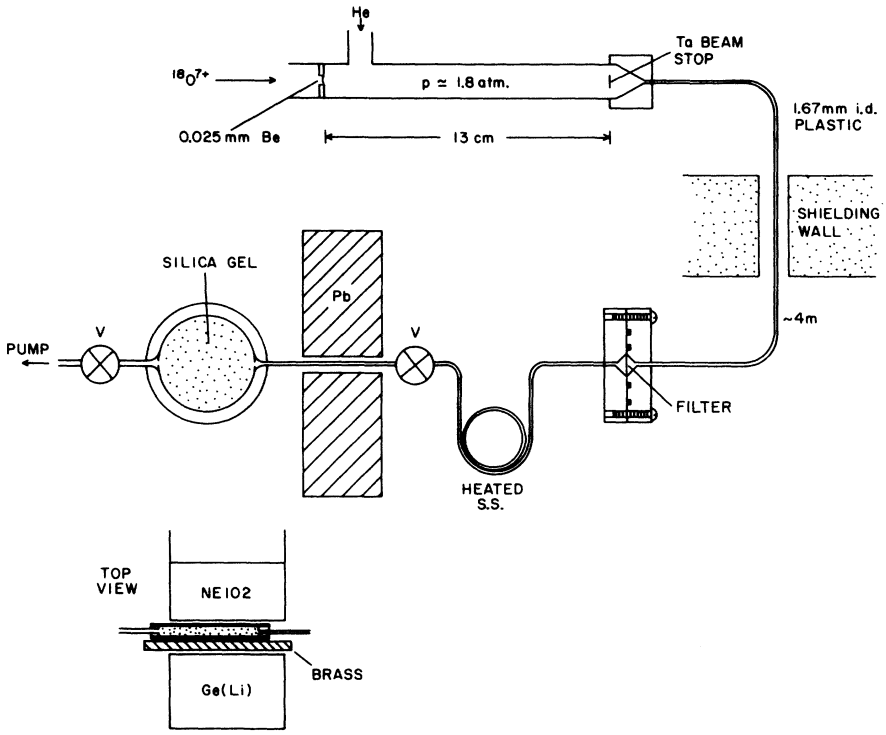

FIG. 2. Schematic diagram of apparatus employed in the study of ^{21}O β decay.

efficiency were used for the γ-γ coincidence measurements. Their relative efficiencies versus γ-ray energy were determined with sources of ^{56}Co, ^{152}Eu, and ^{228}Th. Pb shielding was provided to keep the detectors from seeing the γ radiations from the filter and the stainless steel trap. The room background radiation was minimized by surrounding the detectors with Bi and Fe bricks of >5 cm thickness. All of the electronic components in the counting system were of standard design.

III. EXPERIMENTAL RESULTS AND ANALYSIS

A. Yield curves

The relative yields of the various reaction products were measured using a 2.1-mg/cm^2-thick Be foil and a continuous flow of helium at a pressure of 1.7 atm. Data were acquired at 10-MeV intervals over the range of ^{18}O bombarding energies of 70 to 110 MeV, at beam currents of ~40 particle nA. Typical measurements lasted for about 30 min and yields were normalized to the beam current integrator charge. The experimental arrangement was essentially that of Fig. 2 but with the fluorine trap removed to allow the collection of the fluorine radioactivities and using two large Ge(Li) detectors in order to increase the efficiency.

For each bombarding energy the intensities of the various γ-ray lines of the daughter products were extracted. Known β- and γ-branching ratios[14,15] were then used to calculate the total activity of the parent nuclei. The results are shown in Fig. 3, where we have used the present conclusions on the $^{21}O \rightarrow {}^{21}F$ β decay to determine the relative ^{21}O yield. In Fig. 3 those nuclei thought to be produced predominantly by fusion-evaporation reactions are identified by indicating the light particles in the exit channel. Fusion-evaporation calculations provide a reasonable fit for these cases, but fail to predict a measurable cross section for the $^{9}Be(^{18}O, 2p\alpha)^{21}O$ reaction, probably because of the very large negative Q value. However, the observed ^{21}O cross section exhibits the shape expected for a three-particle emission, but is displaced 10–15 MeV higher in bombarding energy. From these data it was decided that using an ^{18}O bombarding energy of 110 MeV and a thicker Be target should provide an optimum yield of ^{21}O. Based on the target thickness and other factors, the peak reaction cross section is estimated to be ~15 μb, probably reliable to within a factor of 2.

B. γ-ray singles measurements

Figure 4 shows the γ-ray spectrum obtained by bombardment of a 4.2-mg/cm^2 thick Be foil with

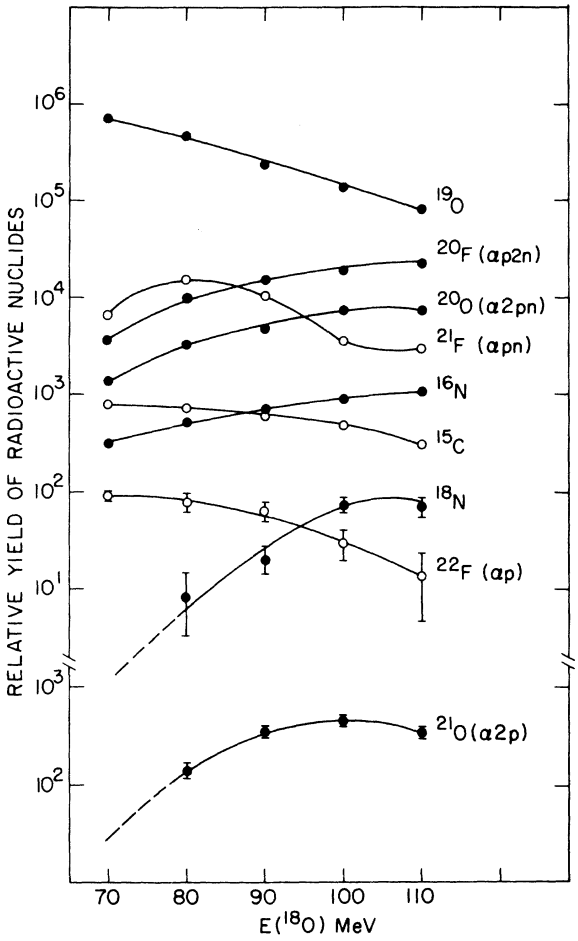

FIG. 3. Relative yields of radioactivities produced from ^{18}O bombardment of a Be foil. Metallic products such as ^{24}Na and ^{28}Al have been removed by filter elements.

108-MeV ^{18}O ions, which corresponds to the peak of the ^{21}O yield observed in Fig. 3 using the 2.1-mg/cm^2-thick Be target. The spectrum presented is actually a composite of the singles spectra measured in the γ-γ and β-γ measurements, to be discussed later, and as such represents ~30 h of running time. These data were measured at a helium flow pressure of 1.8 atm and a beam current of 40 particle nA, using two Ge(Li) detectors of matched gains.

The prominent lines in Fig. 4 are labeled according to the parent nucleus and the known γ-ray energies of the daughter. The identification of ^{21}F lines resulting from the ^{21}O β decay are based largely on the present work, which is found to be in essential agreement with the ^{21}F energy level scheme established previously by Warburton and Olness.[10] The lines from the deexcitation of the ^{21}F 1730-keV state via the 1730 → 0 and 1730 → 280 → 0 cascades are present, although the latter are not discernible at the scale shown in Fig. 4. Also evident are γ rays corresponding to the previously reported[10] decay of ^{21}F states at 1755, 3460, 3518, and 3639 keV. There are, in addition, several "new" lines which are assigned to ^{21}F based on their measured lifetimes and energy production modes, and on additional data from the γ-γ and β-γ measurements.

The data of Fig. 4 were fitted with the peak-fitting program SAMPO[16] to determine the energies and intensities of the lines. Similar fits were also made for several other singles spectra that were acquired. In order to obtain more accurate transition energies, separate runs were made using the mixed-source technique to obtain energies relative to well known lines of ^{56}Co. In particular, the ^{21}O lines near 1730 keV were measured relative to the ^{56}Co line at 1771.350 ± 0.015 keV.[17] Table I summarizes the information thus obtained. The γ rays are placed in the ^{21}F level scheme illustrated in Fig. 1.

With respect to the ^{21}F description given in Fig. 1 and Table I, the excitation energies and γ-decay modes for the 1730- and 1755-keV states are in excellent agreement with the previous conclusions of Warburton and Olness,[10] who quoted excitation energies of 1729.6 ± 1.0 keV and 1754.9 ± 0.7 keV and γ-branching ratios for the 1730-keV state of 1730 → 0 (82%) and 1730 → 280 (18%). Excitation energies of 3450, 3507, and 3629 keV (all with an uncertainty of ±15 keV) were previously reported for the triplet of states near E_{exc} ~ 3.5 MeV, from the t,p studies of Hinds *et al.*[9] While consistently low by ~11 keV, the agreement with the present values is well within the quoted error limits.

For the 3460-keV state, Warburton and Olness[10] reported branches of 3460 → 0 (20 ± 8%), 3460 → 280 (30 ± 12%), and 3460 → 1730 (50 ± 20%), while for the 3639-keV state they observed only a 3639 → 1755 branch. Both are in excellent agreement with the present, more precise, results. However, for the 3518-keV level they reported branchings of 3518 → 0 (50 ± 20%) and 3518 → 280 (50 ± 20%); the present experiment agrees on the ground-state branch but indicates that the only other major branch is the 3518 → 1730 transition. The previous studies of ^{21}F employed the $^{19}F(t,p\gamma)^{21}F$ reaction,[10] where the transitions from the 3460- and 3518-keV states are Doppler-broadened by 10–20 keV, while the proton groups were not resolved by the particle detector. The most likely explanation for the above discrepancy is that some intensity belonging to the 3639 → 280 transition was erroneously assigned to a nonexistent 3518 → 280 transition, while the 3518 → 1730

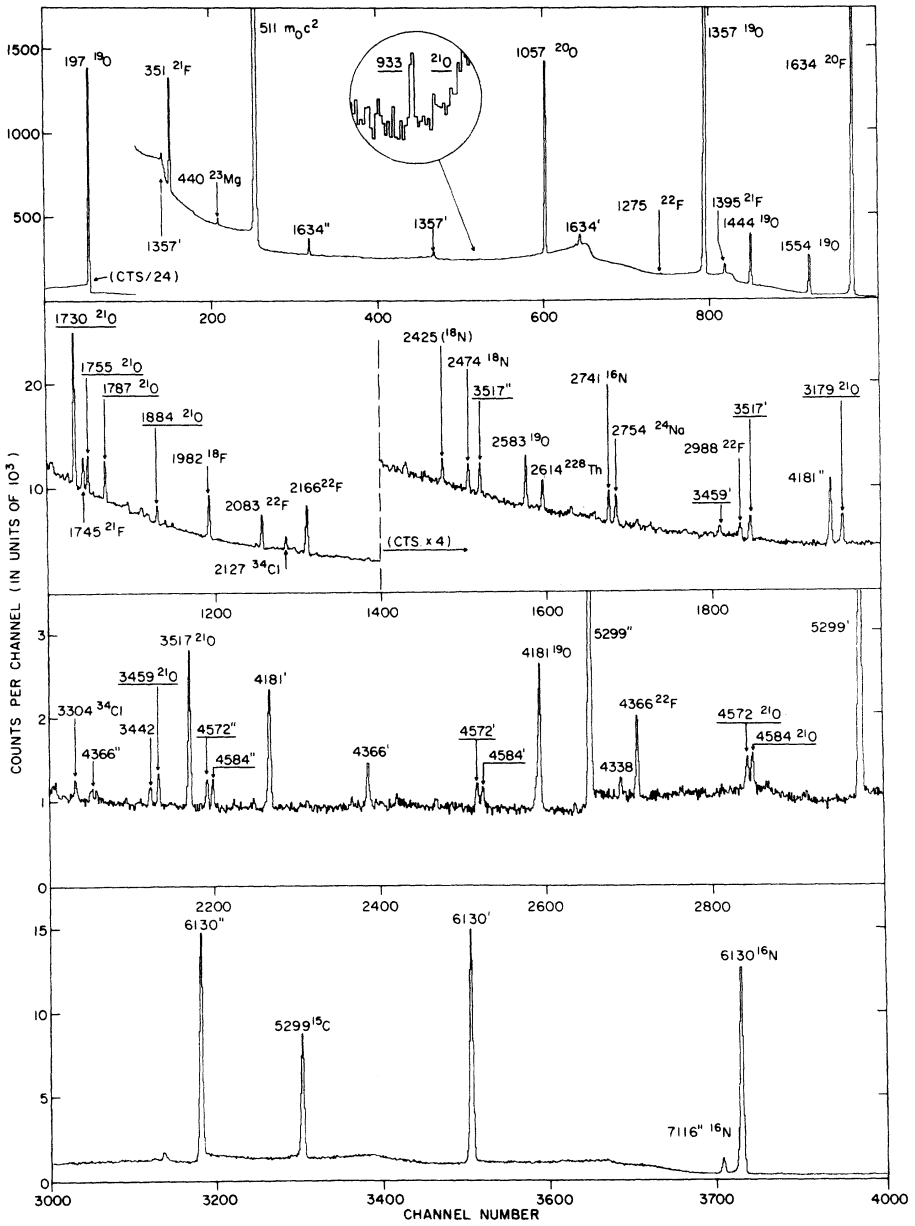

FIG. 4. Spectrum of delayed γ rays resulting from 108-MeV ^{18}O bombardment of a Be foil. Prominent lines are identified according to the radioactive parent nuclide and the energy (in keV) of the deexcitation γ rays of the daughter. The ^{21}F γ rays first observed in the present study of ^{21}O β decay are underlined.

transition was simply not resolved from the stronger 3460 → 1730 → 0 cascade.

The γ-ray data of Fig. 4 also suggest some new information on ^{18}N decay, the ^{18}N presumably being formed in the reaction ^{9}Be(^{18}O, $p2\alpha$)^{18}N. ^{18}N is known to β decay to the 4456 keV ($J^\pi = 1^-$) state of ^{18}O with a 0.63-sec half-life, giving rise to ^{18}O γ rays of 2473, 1982, 1652, and 821 keV. Also evident in Fig. 4 is a 2425-keV γ ray of a similarly short half-life, which probably arises from a previously unreported β branch to the 6882-keV level of ^{18}O, which is known to deexcite via a 6882 → 4456 transition. We have indicated this tentative identification in Fig. 4, noting that confirmation must await the results of additional measurements in progress at this laboratory. If the 6882-keV level of ^{18}O is, in fact, $J^\pi = 0^-$, this would fix the spin-parity of ^{18}N as $J^\pi = 1^-$.

TABLE I. ^{21}F γ rays observed in the β decay of ^{21}O. Uncertainties in the least significant figure are given in parentheses. Excitation energies have been corrected for nuclear recoil.

Transition $E_i \rightarrow E_f$ (keV)	E_γ (keV)	I_γ rel.	Branching ratio (%)	E_{exc} (keV)
280 → 0	280.1(1)	324	100	280.0(1)
1730 → 0	1730.28(8)	1000	82	1730.36(8)
→ 280	1450.5(2)	216	18	
1755 → 0	1754.74(8)	248	100	1754.82(8)
3460 → 0	3459.38(13)	65	24	3459.65(10)
→ 280	3179.43(10)	115	43	
→ 1730	1729.2(N) [a]	90	33	
3518 → 0	3517.40(10)	338	52	3517.66(10)
→ 1730	1787.16(8)	311	48	
3639 → 1755	1884.01(9)	150	100	3638.92(12)
4572 → 0	4572.2(4)	104	45	4572.4(4)
→ 3639	933.2(3)	127	55	
4584 → 0	4583.5(3)	116 (±12) [b]	100 (±2) [b]	4584.1(4)

[a] Nominal value, computed from $E_i - E_f$.
[b] Error applies to all numbers in this column.

C. γ-γ coincidence measurements

Coincidence relationships among the ^{21}F γ rays were established using two Ge(Li) detectors in a geometry identical to that used for the yield curve measurements, but without any intervening absorber material. The measurement involved a total of 50 h of bombardment with a 108-MeV beam of ^{18}O at an average current of 40 particle nA. Coincident events, as established by conventional circuitry with a time resolution of ~50 ns, were stored on magnetic tape for later analysis. Approximately half of the coincidence data were obtained concurrently with the half-life measurements, described in a following section. That measurement was then extended with continuous operation in order to improve the statistics. In a subsequent off-line analysis, gates were set on the γ-ray peaks observed by each detector in order to display the coincident γ spectrum of the other: The detector gains were adjusted so that the pairs of spectra thus obtained could be added directly.

A portion of the data is shown in Fig. 5. The uppermost plot, Fig. 5(a), shows the sum of spectra measured in coincidence with 1755- and 1884-keV γ rays, illustrating their mutual coincidence, and coincidence also with a 933-keV line, resulting from the 4572 → 3639 → 1755 → 0 cascade. These data clearly establish the placement of the 3639- and 4572-keV levels, and in conjunction with the energy measurements of Table I determine their excitation energies quite accurately. The identification of the 4572 → 0 transition is then confirmed, in part, on the basis of the excellent agreement between the excitation energies deduced from the deexcitation routes.

Figure 5(b) illustrates the doublet nature of the 1730-keV γ ray. In coincidence with the 1730-keV gate, one sees the expected 3518 → 1730 cascade and, in addition, a 1730-keV peak corresponding to the unresolved members of the 3460 → 1730 → 0 cascade. The intensity of the 3460 → 1730 branch (Table I and Fig. 1) is derived from the relative intensities of the 1730- and 1787-keV lines as observed in Fig. 5(b) and also from additional results from gates set on extended regions of the 1730- and 1787-keV Compton distributions.

The lowest curve [Fig. 5(c)] illustrates the 1730 → 280 cascade, observed in coincidence primarily with the 1787-keV 3518 → 1730 transition. The fact that the 1730-keV line is twice the intensity of the 1787-keV line indicates again the presence of the energy-redundant 3460 → 1730 → 0 cascade.

Similar spectra constructed for the other γ rays of ^{21}F serve to confirm *all* of the coincidence relationships which should be expected from the level scheme presented in Fig. 1. One can therefore proceed to the determination of the ^{21}O β branching with reasonable confidence in the structure of the daughter nucleus.

D. Further measurements on the ^{19}F(t,$p\gamma$)^{21}F reaction

In the preliminary measurements on ^{21}O β decay, where the ratio of peak-to-background intensities was not nearly as good as that exhibited in Fig. 4, the only clearly discernible ^{21}F γ rays

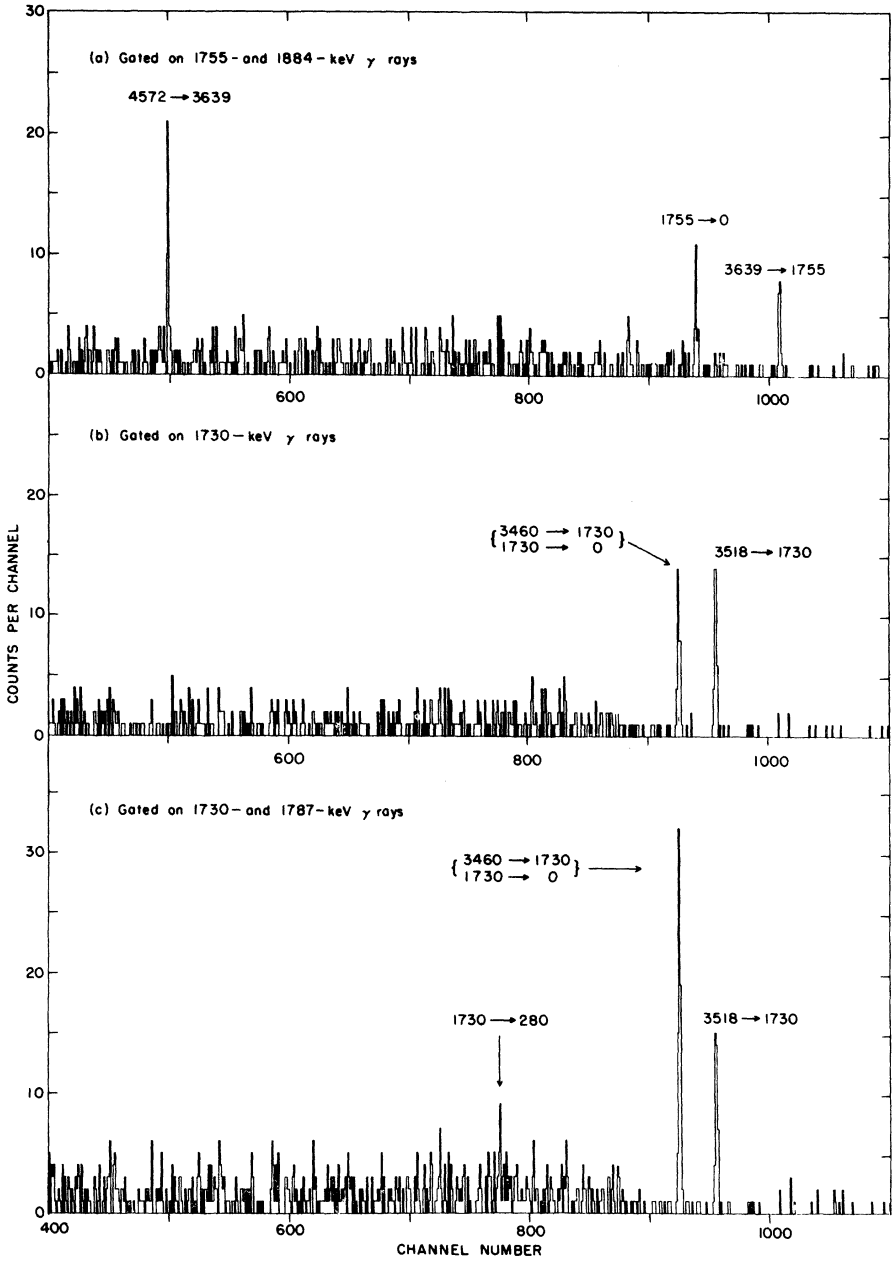

FIG. 5. Coincidence data illustrating γ-γ coincidence relationships among some of the deexcitation γ rays of ^{21}F resulting from ^{21}O β decay.

which could be unambiguously associated with previously known transitions were those of energies 1730 and 1755 keV. In order to check this identification, the ^{19}F$(t, p\gamma)^{21}$F reaction was reexamined to provide more accurate results.

Tritons from the 3.5-MV Van de Graaff bombarded a 500-μg/cm^2-thick target of SrF_2, evaporated onto a 0.25-mm-thick Ta backing. The target was set at an angle of 45° relative to the beam direction, and γ rays were observed by a Ge(Li) detector (19% efficiency) set at an angle of $\theta = 90°$, with an uncertainty in this angular setting of $\pm 0.25°$. The spectrum in the region of interest exhibited a Doppler broadened peak at 1730 keV and a sharp peak at 1755 keV, consistent with the previous lifetime information on these states. (See, for example, Fig. 4 of Ref. 10.)

γ spectra were recorded for triton energies of

2.0, 2.5, and 3.0 MeV, at a dispersion of 0.22 keV/channel, with a ^{56}Co source located on the γ-detector axis providing reference points for the energy calibration. Peak positions were determined by fitting Gaussian shapes to the observed lines, and then fitting a third-order polynomial function to obtain an accurate energy calibration. The results establish the ^{21}F γ-ray energies ($E_{\gamma 0}$) as 1730.05 ± 0.25 keV and 1754.81 ± 0.05 keV, as determined primarily with reference to the nearlying 1771.350 ± 0.015 keV line[17] of ^{56}Co. Second-order Doppler corrections have been incorporated in the value given for the 1730-keV line.

The uncertainty in the 1730-keV energy is due primarily to the uncertainty in θ, since the measured energy is given by $E_\gamma = E_{\gamma 0}(1 + \langle\beta_z\rangle \cos\theta)$. Estimates of $\langle\beta_z\rangle$ for the 1730-keV line were obtained from additional measurements at $\theta = 0°$ and 90°, and have been incorporated in the quoted error for $E_{\gamma 0}$. These values are considerably more accurate than those obtained in the previous $(t, p\gamma)$ measurements,[10] which they now supersede. While both results are in agreement with the values from the present β-decay studies, the new value for the 1755-keV line is the most accurate measurement yet reported.

E. ^{21}F excitation energies

With our new results on the ^{21}F transition energies it becomes possible to set forth the ^{21}F level placement with considerably greater accuracy than was previously possible. These conclusions are summarized in Table II. The first column of the table is derived from the excitation energies reported by Hinds *et al.*[9] from ^{19}F$(t, p)^{21}$F measurements. Their quoted energies have been multiplied by the constant factor 1.0030, effectively renormalizing their energy calibration in order to bring it into better accord with the recent more precise results of Ge(Li) spectroscopy. The third column shows the results of the Ge(Li) measurements of Warburton and Olness[10] in their ^{19}F$(t, p\gamma)^{21}$F studies. Their quoted values for the 1730- and 1755-keV states are superseded by the more accurate remeasurement undertaken in the present studies, as indicated. The present results from studies of the ^{21}O β de-

TABLE II. ^{21}F excitation energies from various sources. Energies are given in keV, with uncertainties in the least significant figure given in parentheses. L values deduced in the t, p reaction are also indicated.

^{19}F(t, p)[a]	$[L]$[b]	^{19}F(t, p)[c]	^{21}O $\xrightarrow{\beta}$ ^{21}F	Adopted
0	[2]			
281	[0]	279.92(6)	280.0(1)	279.92(6)
1103		1100.9(20)		1100.9(20)
1732		1730.13(25)[d]	1730.36(8)	1730.34(8)
1756		1754.89(5)[d]	1754.82(8)	1754.86(5)
2040		2040.0(20)		2040.0(20)
2071		2070.0(20)		2070.0(20)
3460	[2]		3459.65(10)	3459.65(10)
3518	[2]		3517.66(10)	3517.66(10)
3640	[(3)]		3638.92(12)	3638.92(12)
3955				3966(2)
3996				3996(2)
4064				4064(2)
4172				4172(2)
4451				4451(2)
			4572.4(4)	4572.4(4)
4582	[2]		4584.1(4)	4584.1(4)
4669				4669(2)
4924				4924(2)
5029				5029(2)
5079				5079(2)
(all ± 10)				

[a] Values tabulated are 1.003 × values given in Ref. 9.
[b] References 9 and 18.
[c] Reference 10.
[d] Present remeasurement, including correction for nuclear recoil.

cay are given in the fourth column. There is clearly excellent agreement among the three sets of data, and thus we adopt the values given in the last column. Although the accuracy quoted in the t,p results of Hinds *et al.* is only ±10 keV, it is well known that such particle studies have a much better accuracy in the determination of the relative level spacings. In view of the truly excellent agreement obtained with the recalibration procedure used, we estimate a probable error of ±2 keV for the renormalized excitation energies, as indicated.

A further useful piece of evidence from the comparisons shown in Table II is the conclusion that the $E_x = 4584$-keV state observed in ^{21}O β decay is the $L = 2$ state populated in the (t,p) reaction,[9,18] which allows the immediate conclusion that $J^\pi = (\frac{3}{2},\frac{5}{2})^+$.

F. ^{21}O Half-life measurement

For the measurement of the half-life of ^{21}O the counting cycle consisted of a 3 sec flow period with the valves open to allow transfer of activity from the production cell (see Fig. 2), the closure of the valves followed by a 0.1-sec pause for pressure equilibration, and finally a 12.8-sec counting period. Data were obtained from two Ge(Li) detectors placed on either side of the counting cell. γ-ray spectra were collected from each detector in eight sequential 1.6-sec time bins.

The decay curves for the γ rays associated with the ^{21}O decay are shown in Fig. 6. Similar curves for γ rays from the ^{19}O and ^{20}O decays were extracted from the data to check for electronic dead time corrections and systematic errors. Using the values[15] for ^{19}O [$T_{1/2} = 26.91(8)$ sec] and for ^{20}O [$T_{1/2} = 13.57(10)$ sec] as standards, the rate-dependent change in dead time was found to vary by $2.5 \pm 0.3\%$ from the first to last time bin. When this correction was applied, the best value extracted for the half-life of ^{21}O was

$$T_{1/2} = 3.42 \pm 0.10 \text{ sec}.$$

The weighted average of similar fits to the four remaining decay curves of Fig. 6 yields the result $T_{1/2} = 3.43 \pm 0.15$ sec, in excellent agreement with the value quoted above. However, the possibility for systematic errors in the peak intensity determinations for these somewhat weaker lines is correspondingly greater, and therefore we adopt the value and uncertainty derived from the analysis of the 1730-keV γ ray.

Examination of data on the other transitions identified in Fig. 4 indicates half-lives in the range specified by $T_{1/2} = 3.5 \pm 1.5$ sec. Thus all of the data are in agreement with their assignment to ^{21}O β decay.

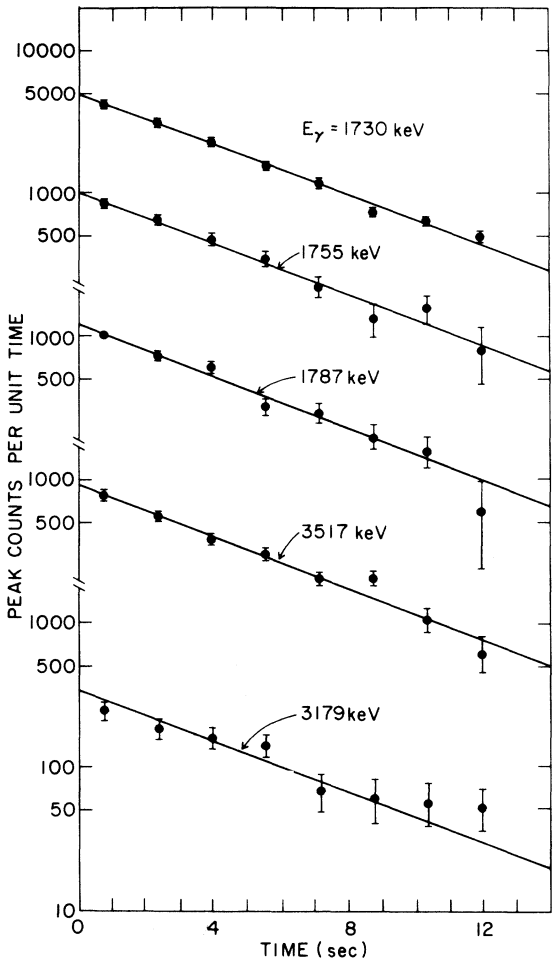

FIG. 6. Data on the half-life of the ^{21}O decay, as observed in the decay curves of various deexciation γ rays of the ^{21}F daughter nucleus. All curves have been fitted to the value $T_{1/2} = 3.42$ sec.

G. β-γ coincidence measurements: ^{21}O mass excess

β-γ coincidence data were collected when using continuous gas flow. The resultant activities, including ^{20}O, ^{19}O, ^{16}N, ^{15}C, ^{20}F, and ^{18}N, in addition to the ^{21}O, spanned a wide range of known[15] β decay energies, and thus provided a precise internal calibration of the β detector for end-point energies of 2.76–9.40 MeV. As illustrated in Fig. 7, the shape of the β spectrum in coincidence with 1634-keV γ rays from the ^{20}F decay was taken as the "standard" shape and used in a conventional stretch fitting analysis.[19] Two mass measurements of ^{21}O were possible: one with β rays in coincidence with 1730-keV γ rays, and the other with β's in coincidence with the 1787- and 3518-keV γ rays from the 3518-keV level. The weighted mean value of these results was

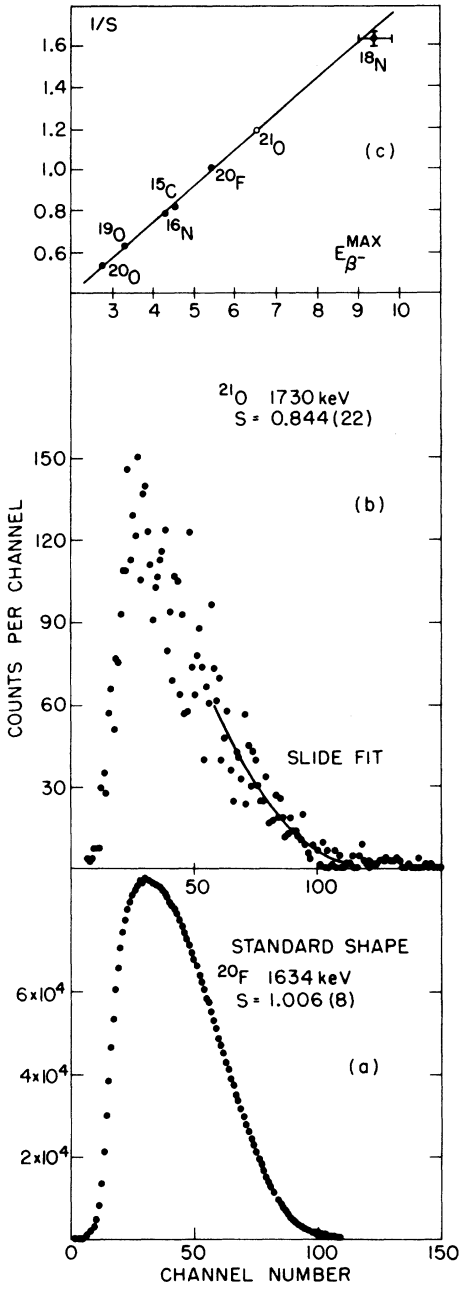

FIG. 7. Data illustrating the determination of the ^{21}O mass excess. Curve (a) shows the β-ray spectrum in coincidence with the 1634-keV γ ray in ^{20}F decay, while curve (b) is the spectrum in coincidence with the 1730-keV γ ray from ^{21}O decay. The stretch factors S required to fit these data with a standard β-ray spectrum shape are indicated. Curve (c) is a plot of the values of $1/S$ determined for various β-ray transitions observed (simultaneously) in the present experiment. A linear fit to these data established the ^{21}O (1730 keV) β end point, and thus the ^{21}O mass excess.

$Q_{\beta^-} = 8152 \pm 175$ keV.

Since the known mass excess[6] of ^{21}F is -47 ± 7 keV, the mass excess of ^{21}O is therefore 8105 ± 175 keV, which is in excellent agreement with the more accurate mean value of 8126 ± 51 keV derived from the two reported nuclear reaction measurements[3-5] discussed in the Introduction.

H. Experimental summary: ^{21}O decay scheme

The foregoing experimental results have been summarized partially in the energy level scheme for ^{21}F shown in Fig. 1; the complete β-decay scheme of ^{21}O is given in the left-hand side of Fig. 8. The latter figure presents the half-life, total decay energy (from reaction Q values), β-ray branching ratios I_β (in percent) to ^{21}F states at 1730, 3460, 3518, (3639), 4572, and 4584 keV, and the γ-ray branching ratios measured for the various ^{21}F states. Also included in the left-hand side of Fig. 8 is a column of total feeding I_F (in percent) of the ^{21}F states by both β and γ rays. ^{21}O β-ray branches and calculated experimental logft values are presented in Table III. This decay scheme is compared with theory in the next section.

IV. SHELL MODEL CALCULATIONS

Previously, Lanford and Wildenthal[7] used the Preedom-Wildenthal[20] effective interaction to calculate logft values for the β decay of ^{21}O to the ground and three excited states of ^{21}F. We have used the effective interaction of Chung and Wildenthal,[21] obtained by fitting energy level data derived from the spectra of the $A = 17-24$ nuclei, to provide wave functions in an $(sd)^5$ model space. The high quality of the fit to energy level data for the Chung-Wildenthal interaction gives confidence in the predictions of the model for the spin of the ^{21}O ground state and for the positive-parity spectrum of ^{21}F at low excitation energy. The ground state of ^{21}O is predicted to have $J^\pi = \frac{5}{2}^+$; a $\frac{1}{2}^+$ first excited state of ^{21}O is predicted at 1.47 MeV. In ^{21}F many $\frac{3}{2}^+$, $\frac{5}{2}^+$, and $\frac{7}{2}^+$ levels are predicted to be energetically available to the allowed β decay of ^{21}O. Since only the ground and first-excited states of ^{21}F have unambiguous spin assignments,[14] no definite spin assignments for the ^{21}O ground state or levels in ^{21}F can be made from the experimental data. However, a detailed comparison of the experimentally observed and theoretically predicted β branching ratios and γ-ray intensities allows confident predictions, if not rigorous assignments, to be made for the spins of a number of levels in ^{21}F.

In computing Gamow-Teller matrix elements for

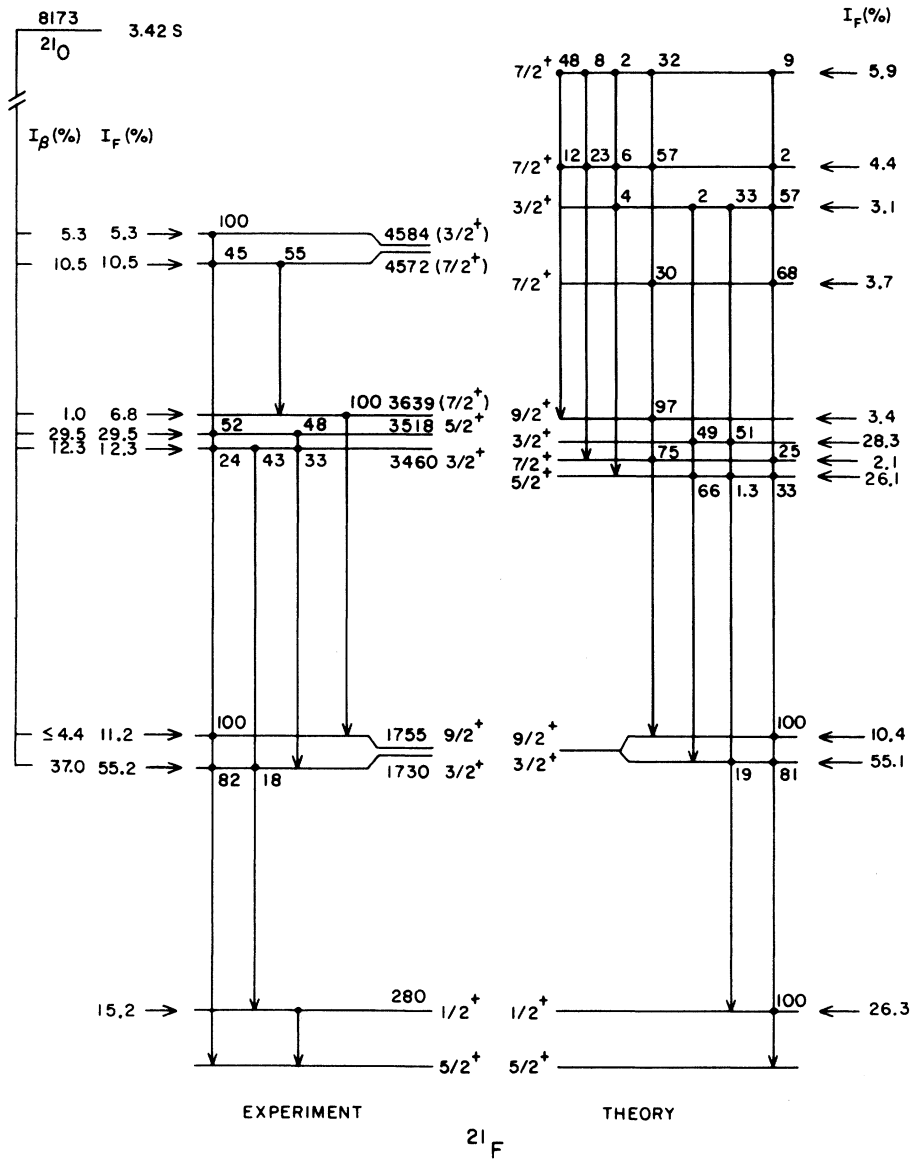

FIG. 8. Comparison of theoretical and experimental β and γ decay schemes for $^{21}O \rightarrow {}^{21}F$. The numbers I_F on the two sides represent the percentage of the total β decay passing through the level in question (the sum of direct feeding plus cascade γ rays). On the left the numbers I_β are percentages of direct β decay determined experimentally.

the β decay of ^{21}O, both free nucleon and empirically renormalized[22] one-body Gamow-Teller matrix elements are used. Similarly, in computing $B(M1)$ values, two sets of single particle matrix elements[21] are used.

A. Results

The details of the calculated β-decay scheme for ^{21}O are given in Table IV. Comparison between theory and experiment is made in Fig. 8, which includes the spectrum of ^{21}F levels relevant to the β decay of ^{21}O, γ-ray branching ratios for these levels, and the percentage of the β decay passing through each level (direct plus cascade). Calculated electromagnetic transition strengths for the lowest positive parity states of ^{21}F are given in Table V. The assignments of $\frac{3}{2}^+$ and $\frac{9}{2}^+$ to the 1730- and 1755-keV levels, respectively, are clear. Strong β branches are predicted to the $\frac{3}{2}^+_2$ and $\frac{5}{2}^+_2$ model states in the region of 3.5 MeV, and are observed to a pair of levels at 3460 and 3518 keV which have $(\frac{3}{2}^+, \frac{5}{2}^+)$ assignments. A $\frac{3}{2}^+$ assignment to the 3460-keV level is preferred on account of the large γ branch to the

TABLE III. β-ray branches and logft values in the decay of ^{21}O ($J^\pi = \frac{5}{2}^+$, $T_{1/2} = 3.42 \pm 0.10$ sec, $Q_\beta = 8173 \pm 51$ keV). Uncertainties in the least significant figure are indicated in parentheses.

State of ^{21}F (keV)	J^π	β-ray branch (%)	logft
1730	$\frac{3}{2}^+$	37.0(12)	5.24(2)
1755	$\frac{9}{2}^+$	≤ 4.4	≥ 6.2
3460	$\frac{3}{2}^+, \frac{5}{2}^+$	12.3(12)	5.09(4)
3518	$\frac{3}{2}^+, \frac{5}{2}^+$	29.5(12)	4.69(2)
3639		1.0 ± 1.0	$6.1^{+?}_{-0.3}$
4572		10.5(12)	4.63(5)
4584	$\frac{3}{2}^+, \frac{5}{2}^+$	5.3(12)	4.92(9)

$\frac{1}{2}^+$ level at 280 keV; theory and experiment agree well on the two major branches of the $\frac{3}{2}^+_2$ level, but the predicted ground state branch is much too weak. The $\frac{5}{2}^+_2$ model state is predicted to decay to the $\frac{5}{2}^+_1$ and $\frac{3}{2}^+_1$ levels and can be identified with the 3518-keV level; only a very weak branch of ~1% is predicted to the $\frac{1}{2}^+_1$ level.

If the 3639-keV level is populated directly in β decay, it is natural to identify it as the first $\frac{7}{2}^+$ level. The direct β branch to the $\frac{7}{2}^+_1$ level is predicted to be only 0.5%, which is in agreement with the measured branch of 1 ± 1%. The only observed γ decay from the 3639-keV level is to the $\frac{9}{2}^+$ level at 1755 keV, in agreement with the dominant decay mode predicted for the $\frac{7}{2}^+_1$ level. In Tables IV and V we have tentatively identified the $\frac{7}{2}^+_1$ model state with the 3639-keV level. However, if the 3639-keV level is not directly populated in the β decay, a possibility not ruled out by the data, its spin and parity are much less restricted. In fact, the properties of the $\frac{9}{2}^+_2$ model state match well with those known for the 3639-keV level, and several spin assignments with negative parity are, in principle, possible.

The next group of positive parity levels predicted by the shell model are $\frac{9}{2}^+_2$, $\frac{1}{2}^+_2$, and $\frac{3}{2}^+_3$ lev-

TABLE IV. Shell-model decay scheme for ^{21}O β decay.

J^π	E_x[a] (keV)	E_β (max) (keV)	$ft_{1/2}$[b] (sec)	$ft_{1/2}$[c] (sec)	f[d]	$t_{1/2}$[b] (sec)	Branch[b] (%)
$\frac{5}{2}^+$	0	8173	4.686(7)[e]	5.859(6)[e]	5.764(4)[e]	813.0	0.4
	3518	4655	5.610(4)	5.594(4)	4.227(3)	13.27	25.6
	4400	3773	3.538(5)	9.697(5)	1.631(3)	216.9	1.6
	4930	3243	1.103(6)	8.923(5)	8.289(2)	1331	0.3
	5530	2643	1.454(5)	9.804(4)	3.369(2)	431.6	0.8
	6120	2053	1.481(6)	1.358(6)	1.134(2)	13060	0.0
	6330	1843	4.843(4)	3.693(4)	7.177(1)	674.8	0.5
$\frac{3}{2}^+$	1730	6443	2.688(5)	3.174(5)	1.892(4)	14.21	23.9
	3460	4713	5.378(4)	6.679(4)	4.472(3)	12.03	28.2
	3920	4253	1.031(6)	5.670(5)	2.802(3)	368.0	0.9
	4800	3373	1.068(5)	8.660(4)	9.875(2)	108.2	3.1
	5440	2733	1.081(6)	6.166(5)	3.899(2)	2773	0.1
$\frac{7}{2}^+$	3640	4533	2.583(6)	3.010(6)	3.744(3)	689.9	0.5
	4400	3773	1.484(5)	1.228(5)	1.631(3)	90.99	3.7
	5050	3123	5.462(4)	4.946(4)	7.015(2)	77.86	4.4
	5570	2603	1.828(4)	1.544(4)	3.152(2)	57.99	5.9
	6130	2043	2.122(5)	2.098(5)	1.110(2)	1890	0.2
			$t_{1/2}$ (total) = 3.39[b] (3.46)[c] sec				

[a] Calculated excitation energies are used except for the $\frac{5}{2}^+_2$, $\frac{3}{2}^+_1$, $\frac{3}{2}^+_2$, and $\frac{7}{2}^+_1$ levels. For these levels the correspondences made in Fig. 8 are assumed and the experimental excitation energies are used.

[b] Calculated using the empirical single-particle Gamow-Teller matrix elements of Ref. 22.

[c] Calculated using the free nucleon single-particle Gamow-Teller matrix elements.

[d] The phase space factor is calculated using the tables of D. H. Wilkinson and B. E. F. Macefield, Nucl. Phys. A232, 58 (1974) and includes the outer radiative correction of order α. To follow as closely as possible Brown, Chung, and Wildenthal (Ref. 22), we write

$$ft_{1/2} = \frac{C(1-4.00\times10^{-4}Z - 3.60\times10^{-6}Z^2)}{M(F)^2 + (C_A/C_V)^2 M(GT)^2},$$

where $C = 6177$ and $|C_A/C_V| = 1.251$. The Z dependent terms represent the energy-independent higher order radiative corrections of order $Z\alpha^2$ and $Z^2\alpha^3$.

[e] The numbers in parentheses refer to the exponent.

TABLE V. Electromagnetic transition strengths[a] in ^{21}F.

$J_i \rightarrow J_f$	E_i (keV)	E_f (keV)	$B(M1)$[b,c] (W.u.)		$B(E2)$[b,d] (W.u.)	δ[c]	τ
$\frac{1}{2} \rightarrow \frac{5}{2}$	280	0			21.6		6.4 ns
$\frac{3}{2} \rightarrow \frac{5}{2}$	1730	0	0.93	(1.01)	1.0	−0.021	
$\rightarrow \frac{1}{2}$		280	0.371	(0.339)	7.1	+0.073	5.3 fs
$\frac{9}{2} \rightarrow \frac{5}{2}$	1755	0			5.5		2.6 ps
$\frac{3}{2} \rightarrow \frac{5}{2}$	3460	0	0.000 21	(0.000 92)	0.14	+1.06	
$\frac{1}{2}$		280	0.145	(0.146)	0.33	−0.056	
$\frac{3}{2}$		1730	0.875	(0.916)	4.2	−0.044	3.5 fs
$\frac{5}{2} \rightarrow \frac{5}{2}$	3518	0	0.033 7	(0.035 3)	0.01	+0.024	
$\frac{1}{2}$		280			0.14		
$\frac{3}{2}$		1730	0.621	(0.591)	0.77	+0.020	7.9 fs
$\frac{7}{2} \rightarrow \frac{5}{2}$	3639	0	0.065 3	(0.055 4)	1.0	+0.17	
$\frac{3}{2}$		1730			6.6		
$\frac{9}{2}$		1755	1.45	(1.58)	0.07	+0.005	2.4 fs
$\frac{9}{2}$ $\frac{5}{2}$	(3960)[e]	0			0.32		
$\frac{9}{2}$		1755	0.026 7	(0.022 7)	0.81	+0.14	
$\frac{7}{2}$		3639	0.188	(0.191)	0.12	+0.003	108 fs
$\frac{1}{2}$ $\frac{1}{2}$	(3960)[e]	280	0.133	(0.186)			
$\frac{3}{2}$		1730	1.27	(2.58)	2.58	+0.037	1.5 fs
$\frac{7}{2}$ $\frac{5}{2}$	(4400)[f]	0	0.013 9	(0.015 9)	0.51	+0.31	
$\frac{9}{2}$		1755	0.028 6	(0.022 1)	0.08	+0.050	
$\frac{7}{2}$		3639	0.052 8	(0.064 5)	0.02	+0.001	
$\frac{9}{2}$		(3960)[e]	0.414	(0.465)	1.52	+0.010	16.8 fs

[a] Included are positive parity levels below 3.64-MeV excitation energy for which we have made assignments in the text. The $\frac{1}{2}^+_2$ and $\frac{9}{2}^+_2$ levels are included because the predicted decay schemes are simple and because one or perhaps both may be identified with states at 3.96 and 3.98 MeV (a γ ray from the 3.96-MeV level is reported in Ref. 10).

[b] The Weisskopf unit is that of S. J. Skorka, J. Hertel, and T. W. Retz-Schmidt, Nucl. Data A2, 347 (1966).

[c] The empirical single-particle $M1$ matrix elements of Chung and Wildenthal (Ref. 21) are used in calculating $B(M1)$ values. The numbers in parentheses are calculated using bare nucleon g factors.

[d] Effective charges of $1.5e$ and $0.5e$ for protons and neutrons, respectively, are used in calculating $B(E2)$ values.

[e] Lowest possible excitation energy given the assignments made in the text for levels with excitation energies below 3.7 MeV.

[f] Excitation energy taken from shell model calculation.

els at 3.60, 3.76, and 3.92 MeV, respectively. They play little part in the β decay, although some γ rays from the higher $\frac{7}{2}^+$ levels are expected to cascade through the $\frac{9}{2}^+_2$ level to the $\frac{9}{2}^+_1$ level. Candidates for these levels do not occur below 3.96 MeV—except that the 3639-keV level discussed above could conceivably have $J^\pi = \frac{9}{2}^+$; the 3.96-MeV level has been observed[10] to decay to the $\frac{3}{2}^+_1$ level, and this is predicted to be the dominant decay mode of the $\frac{1}{2}^+_2$ level. For levels above 4 MeV the comparison of theory with experiment is necessarily more qualitative in nature and we do not attempt to make definite correspondences. Table IV and Fig. 8 show that an appreciable percentage of the β decay should go to $\frac{7}{2}^+$ levels at higher excitation energies. The observation of

an excess of γ rays going through the $\frac{9}{2}_1^+$ level over those going through the $\frac{7}{2}_1^+$ level argues for the existence of β branches to such levels. The 4572-keV level is a candidate for identification as one of the higher $\frac{7}{2}^+$ levels. However, this level takes more of the β decay strength than is predicted for the $\frac{7}{2}_2^+$ model state and its γ decay scheme does not resemble that of any of the higher $\frac{7}{2}^+$ states, which are all predicted to have appreciable γ branches to the 1755-keV level and small γ branches to the 3639-keV level. It is possible, by taking linear combinations of the wave functions of the higher $\frac{7}{2}^+$ states, to obtain a wave function which reproduces the observed γ branching ratios of the 4572-keV level, but this wave function then gives much more β strength than is observed. This exercise is perhaps not well advised, since the branching ratios are determined by rather weak $M1$ matrix elements, as typified by the entries in Table V for the $\frac{7}{2}_2^+$ level.

The remaining level observed in the β decay of ^{21}O is the 4584-keV level, which has a $(\frac{3}{2}^+, \frac{5}{2}^+)$ spin-parity assignment. The only theoretical candidate is the $\frac{3}{2}_4^+$ model state, which has about the right β strength (4.1% if the experimental excitation energy is used to calculate the ft value) and is predicted to γ decay predominantly to the ^{21}F ground state.

Finally, we consider the negative parity levels of ^{21}F, the lowest of which are expected to have dominant components corresponding to the coupling of a $p_{1/2}$ proton hole to the 0^+, 2^+, and 4^+ members of the ^{22}Ne ground-state band. We identify the $\frac{1}{2}^-$, $\frac{3}{2}^-$, and $\frac{5}{2}^-$ states with the 1101-, 2040-, and 2071-keV states of ^{21}F, respectively, and expect a $\frac{5}{2}^-$, $\frac{7}{2}^-$ doublet to occur just above 4 MeV in excitation energy. The unique first-forbidden β decay to the $\frac{1}{2}^-$ level is expected to have $\log ft \gtrsim 10$, and thus a negligible β branch. Branches of nonunique first-forbidden decays to the $\frac{3}{2}^-$ or $\frac{5}{2}^-$ states would be less than one percent even for $\log ft$ values as small as 6.8, such as occur[23] in the β decay of ^{11}Be. We estimate that γ branches to the negative parity levels from any of the states populated in the β decay are likely to be very small. Even a $B(E1)$ as large as 10^{-3} W.u. gives a very small branch in almost all cases—15%, 20%, and 8% for $\frac{7}{2}_2^+$, $\frac{7}{2}_3^+$, and $\frac{7}{2}_4^+$, respectively, being by far the largest. There is no evidence in our data for γ rays involving the negative parity levels.

Our overall conclusion regarding the $(sd)^5$ shell model description for the β decay of ^{21}O is that the model works remarkably well. In particular, the measured $(3.42 \pm 0.10$ sec) and predicted (3.39–3.46 sec) values for the half-life of ^{21}O are in excellent agreement. This agreement does not depend on the use of the fitted set of single-particle matrix elements, the free-nucleon set giving an equally good value for the half-life. The theory successfully predicts that the three major β-decay branches should be to the $\frac{3}{2}_1^+$, $\frac{3}{2}_2^+$, and $\frac{5}{2}_2^+$ levels, with an appreciable percentage of the decay, clearly from β branches to $\frac{7}{2}^+$ levels, cascading through the $\frac{9}{2}_1^+$ level. In detail, the agreement is certainly not perfect for either the primary β branches or the γ branches of the 3.5-MeV group of levels. However, the agreement is good considering that the β transitions are hindered considerably with respect to superallowed values and depend crucially, e.g., on the mixing of different supermultiplet symmetries in the wave functions as we elaborate on below.

B. Discussion of the wave functions

The Gamow-Teller operator clearly cannot connect initial and final states which differ in any of the spatial quantum numbers; i.e., in an SU(4)/SU(3) basis it cannot connect configurations with different $[f]$, $(\lambda\mu)$, K, or L. In light nuclei, as a consequence of the strong space-exchange component in the effective central interaction, high spatial symmetries generally dominate the wave functions of low-lying levels. Admixtures of different symmetries are caused by spin-dependent interactions, one of the principal symmetry breaking interactions being the one-body spin-orbit force. Since the highest spatial symmetries $[f]$ for different isospins are usually different, with the obvious exception occurring for $T=0$ and $T=1$ in $A=4n+2$ nuclei, β decay proceeds to small components in the final wave function with symmetry lower than the highest possible. This point is illustrated for ^{21}O and ^{21}F in Table VI, where it may be seen that the admixtures of [221], [2111], and [11111] symmetry in the $T=\frac{3}{2}$ wave functions are small, and that this mismatch alone will cause more than an order of magnitude increase in $ft_{1/2}$ with respect to a case in which there is almost perfect matching of the spatial wave functions in the initial and final states. As Table VII shows, there is a further mismatch in SU(3) symmetries for the ground-state to ground-state transition, which is consequently very strongly inhibited. The [221] (51) $K_L=1$ component in the $T=\frac{3}{2}$ wave function is admixed by the one-body spin-orbit force into the dominant [32] (62) $K_L=0$ component, while the largest components in the $T=\frac{5}{2}$ wave function have $K_L=2$. Since $K_L=1$ and $K_L=2$ cannot occur for the same SU(3) representation, the mismatch in K_L values implies a mismatch in SU(3) symmetries.

Also included in Tables VI and VII (numbers in parentheses) for some states is an analysis of

TABLE VI. SU(4) content (%) for $(sd)^5$ wave functions.

$[f]$ [a] $J_n; T$	[41]	[32]	[311]	[211]	[2111]	[11111]
$\frac{5}{2_1}; \frac{5}{2}$				79.24	20.51	0.26
				(85.49) [b]	(14.39)	(0.12)
$\frac{5}{2_1}; \frac{3}{2}$		64.72	26.82	8.13	0.33	0.00
		(70.91)	(22.19)	(6.60)	(0.30)	(0.00)
$\frac{5}{2_2}; \frac{3}{2}$		50.05	41.44	6.96	1.55	0.00
$\frac{3}{2_1}; \frac{3}{2}$		57.06	35.29	6.84	0.81	0.00
$\frac{3}{2_2}; \frac{3}{2}$		62.73	29.28	6.58	1.37	0.05
$\frac{7}{2_1}; \frac{3}{2}$		51.76	38.03	8.88	1.32	0.00

[a] SU(4) labels are given by $[\tilde{f}]$.

[b] Numbers in parentheses are for the Kuo-Brown interaction (Ref. 24). The others are for the Chung-Wildenthal interaction (Ref. 21).

wave functions computed using the Kuo-Brown interaction.[24] It is known that realistic interactions conserve spatial symmetry somewhat better than the empirical Chung-Wildenthal interaction, and this is evident from Tables VI and VII. Consequently, it is not a surprise that the Kuo-Brown interaction predicts a half-life for ^{21}O of 5.8 sec, which is longer than the Chung-Wildenthal value. Further, the Kuo-Brown predictions for branching ratios for β decay to the $\frac{3}{2_1}^+$, $\frac{3}{2_2}^+$, and $\frac{5}{2_2}^+$ levels of 59.4%, 1.0%, and 11.2% are in poor agreement with the experimental data, thus illustrating the point that data on allowed β decay provides a very useful test of the symmetry breaking characteristics of different effective interactions.

This research was performed under Contract No. DE-AC02-76CH00016 with the Division of Basic Energy Sciences, U. S. Department of Energy.

APPENDIX

The experimental arrangement shown in Fig. 2 resulted from a number of measurements and design considerations. Because the ^{21}O half-life was expected to be 1–3 sec, it was clearly desirable to develop a system in which the target-collector transfer time was correspondingly short. The results of some tests on the transfer system are shown in Fig. 9, which also indicates the arrangement used for these measurements.

With the helium flow set to give a chamber pressure of 1.2 atm, the valve (V) was closed and the gauge pressure (G) was recorded as a function of time. The central curve shows results for the system used in the experiment, with three 0.8-μm pore size biological filter papers installed and with the collector cell loaded with silica gel. The dashed curve shows the results of similar measurements with a "bare system," i.e., with the filter papers and silica gel removed. Clearly, the impedance of the system is not greatly increased by the presence of the filter and collector materials, inasmuch as the time scale is augmented by only ~50%. These measurements used tubing of 1.67 mm i.d. For comparison, the data obtained using 1.14-mm i.d. tubing exhibits a 100%

TABLE VII. SU(3) content (%) for [221] symmetry.

$(\lambda\mu)$ $J_n; T$	(51)	(24)	(32)	(40)	(13)	(21)	(02)
$\frac{5}{2_1}; \frac{5}{2}$	0.97	29.31	23.20	0.09	13.58	7.35	4.73
	(5.78) [a]	(40.03)	(20.92)	(0.22)	(16.09)	(1.90)	(0.50)
$\frac{5}{2_1}; \frac{3}{2}$	6.34	0.49	0.21	0.79	0.05	0.22	0.03
	(5.07)	(0.70)	(0.24)	(0.42)	(0.09)	(0.07)	(0.01)
$\frac{5}{2_2}; \frac{3}{2}$	0.95	3.80	1.56	0.38	0.17	0.06	0.02

[a] Numbers in parentheses are for the Kuo-Brown interaction (Ref. 24). The others are for the Chung-Wildenthal interaction (Ref. 21).

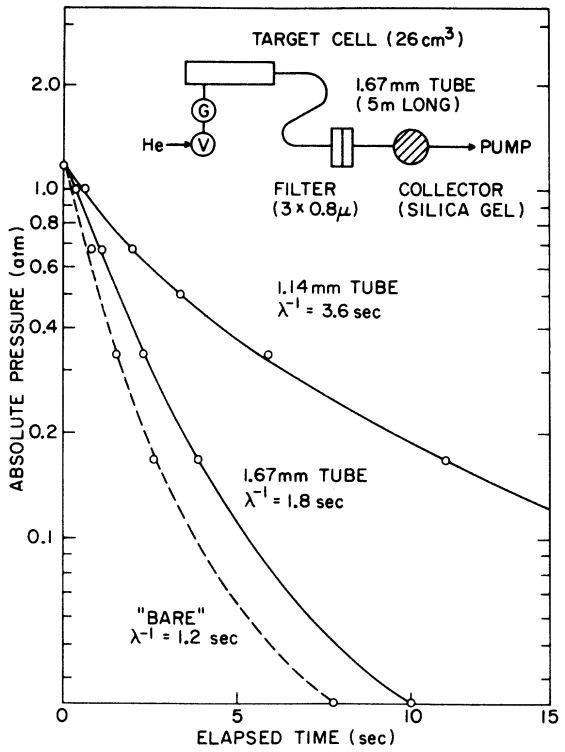

FIG. 9. Gas flow data for the system used in the ^{21}O experiments.

increase in the pump-out time, which corresponds roughly to the 50% decrease in the cross sectional area of the transfer tubing.

The data shown in Fig. 9 have been fitted with the simple functional form

$$P(t) = P_0 e^{-\lambda t} + \text{constant},$$

where $P(t)$ is the absolute pressure and λ^{-1} is a measure of the impedance of the system. The values of λ^{-1} are indicated. The transport velocity is then calculated to be 6.5 m/sec, corresponding to a target-collector transport time of 0.9 sec. With a target-chamber of volume 26 cm^3, these data indicate that >75% of the radioactive products stopped by the helium will be transported to the collector site within 2 sec of their production. The system therefore seems to be appropriate for the study of activities with half-lives as short as 0.5 sec and, in fact, the 0.63-sec activity of ^{18}N was observed quite easily.

Filters

The suggestion that we use biological filters to eliminate metallic radioactive products from the helium flow stream was made by Davids,[12] to whom we are greatly indebted. His design (for another usage) was modified such that the inlet and exit bores to the filter were opened up, by means of conical chambers, to 6 mm diameter at the filter faces (see Fig. 2), thereby reducing the impedance of the filter array by increasing the cross-sectional area available for transmission of gas. A brass screen of 70% transmission placed on the lower-pressure side provided a support for the filter papers.

Measurements carried out using two Ge(Li) detectors to determine the specific radioactivities at the filter and collector sites confirmed that the activity at the collector site due to various metallic products was essentially negligible; the particularly bothersome ^{24}Na activity was reduced to $\lesssim 0.5\%$ of its initial level.

Several different arrangements were tested using filters of pore sizes 0.4, 0.8, and 1.2 μm, both singly and in combinations of two and three pieces. The 0.4-μm filters produced a measurable increase in the transport impedance, while little if any change was noted in the filtering efficiency. Little difference was noted between the 0.8- and 1.2-μm sizes, and the former was therefore selected. The measurements employed three 0.8-μm filters, providing some margin of safety and a negligible increase in transport impedance.

Fluorine traps

It was observed that the radioactivities of the fluorine isotopes ($A = 20$, 21, 22) were trapped out in a short length of steel tubing used in the helium flow line. An effective fluorine "filter" was devised, consisting of a 50-cm long loop of 1.6-mm i.d. stainless steel tubing, which was heated electrically to >100°C. The heat had no measurable impact on the fluorine absorption, but ensured that water vapor was *not* trapped. Measurements indicated that this trapping system removed >80% of the fluorine radioactivity.

Collectors

Molecular sieves, activated charcoal, and silica gel were tried as collectors of the ^{21}O activity; in addition, gases were trapped in stainless steel tubes cooled to liquid-nitrogen and dry-ice temperatures. All of these seemed to work reasonably well. Silica gel was finally used because it was simple to handle and it appeared to have somewhat less affinity for the carbon and nitrogen radioactivities.

*Present address: Shuster Laboratory, Department of Physics, University of Manchester, Manchester M13 9PL, England.

[1]For a review, see D. E. Alburger, D. R. Goosman, C. N. Davids, and J. C. Hardy, in *Atomic Masses and Fundamental Constants 5*, edited by J. H. Sanders and A. H. Wapstra (Plenum, New York, 1976), p. 73.

[2]A. G. Artukh, V. V. Avdeichikov, G. F. Gridnev, V. V. Volkov, and J. Wilczynski, Nucl. Phys. A192, 170 (1972).

[3]G. C. Ball, W. G. Davies, J. S. Forster, and H. R. Andrews, Phys. Lett. 60B, 265 (1976).

[4]G. C. Ball, W. G. Davies, J. S. Forster, H. R. Andrews, D. Horn, and W. McLatchie, Nucl. Phys. A325, 305 (1979). The value given here for the ^{21}O mass excess supersedes that quoted in Ref. 3.

[5]F. Naulin, C. Détraz, M. Bernas, E. Kashy, M. Langevin, F. Pougheon, and P. Roussel, Phys. Rev. C 17, 830 (1978).

[6]A. H. Wapstra and K. Bos, At. Data Nucl. Data Tables 19, 175 (1977).

[7]W. A. Lanford and B. H. Wildenthal, Phys. Rev. C 7, 668 (1973).

[8]G. T. Garvey, W. J. Gerace, R. L. Jaffe, I. Talmi, and I. Kelson, Rev. Mod. Phys. Suppl. 41, S1 (1969).

[9]S. Hinds, H. Marchant, and R. Middleton, Nucl. Phys. 31, 118 (1962).

[10]E. K. Warburton and J. W. Olness, Phys. Rev. C 2, 2235 (1970).

[11]D. R. Goosman, D. E. Alburger, and J. C. Hardy, Phys. Rev. C 7, 1133 (1973).

[12]C. N. Davids, private communication. The system was used for the problem described in Bull. Am. Phys. Soc. 25, 46 (1980), but is not mentioned in that abstract.

[13]G. E. Schwender, D. R. Goosman, and K. W. Jones, Rev. Sci. Instrum. 43, 832 (1972).

[14]P. M. Endt and C. Van der Leun, Nucl. Phys. A310, 1 (1978).

[15]F. Ajzenberg-Selove, Nucl. Phys. A300, 1 (1978); A281, 1 (1977); A268, 1 (1976).

[16]J. T. Routti and S. G. Prussin, Nucl. Instrum. Methods 72, 125 (1969).

[17]C. Van der Leun, R. G. Helmer, and P. H. M. Van Assche, in *Atomic Masses and Fundamental Constants 6*, edited by J. A. Nolen and W. Benenson (Plenum, New York, 1979), p. 502.

[18]P. Horvat, Nucl. Phys. 52, 410 (1964).

[19]D. R. Goosman and D. E. Alburger, Phys. Rev. C 7, 2409 (1973).

[20]B. M. Preedom and B. H. Wildenthal, Phys. Rev. C 6, 1633 (1972).

[21]W. Chung and B. H. Wildenthal (unpublished); W. Chung, thesis, Michigan State University, 1976.

[22]B. A. Brown, W. Chung, and B. H. Wildenthal, Phys. Rev. Lett. 40, 1631 (1978).

[23]D. E. Alburger and D. H. Wilkinson, Phys. Rev. C 3, 1492 (1971).

[24]T. T. S. Kuo and G. E. Brown, Nucl. Phys. 85, 40 (1966).